

# Numerical determination of wind forces acting on structural elements in the shape of a curved pipe

Agnieszka Padewska-Jurczak<sup>\*1</sup>, Piotr Szczepaniak<sup>1a</sup> and Zbigniew Buliński<sup>2</sup>

<sup>1</sup>Department of Mechanics and Bridges, Faculty of Civil Engineering, Silesian University of Technology, Akademicka 5, 44-100 Gliwice, Poland

<sup>2</sup>Institute of Thermal Technology, Faculty of Energy and Environmental Engineering, Silesian University of Technology, Konarskiego 18, 44-100 Gliwice, Poland

(Received September 10, 2018, Revised June 16, 2019, Accepted August 10, 2019)

**Abstract.** This paper reports the study on development and verification of numerical models and analyzes of flow at high speed around structural elements in the shape of a curved pipe (e.g., a fragment of a water slide). Possibility of engineering estimation of wind forces acting on an object in the shape of a helix is presented, using relationships concerning toroidal and cylindrical elements. Determination of useful engineering parameters (such as aerodynamic forces, pressure distribution, and air velocity field) is presented, impossible to obtain from the existing standard EN 1991-1-4 (the so-called wind standard). For this purpose, flow at high speed around a torus and helix, arranged both near planar surface and high above it, was analyzed. Analyzes begin with the flow around a cylinder. This is the simplest object with a circular cross-section and at the same time the most studied in the literature. Based on this model, more complex models are analyzed: first in the shape of half of a torus, next in the shape of a helix.

**Keywords:** finite volume method; finite element method; computational fluid dynamics; fluid–structure interaction; wind engineering; wind action; water slide

## 1. Introduction

Structural elements with circular cross-sections and nontypical shapes are applied in engineering on a large scale. They can be found among others in objects such as follows:

- urban structures: e.g., elements of bridges, roofs, noise barriers, masts;
- industrial structures: e.g., pipelines; and
- recreational structures: e.g., water slides, carousels, roller coasters, and so on.

So far, methods or algorithms for the design of structures and/or construction elements of a circular cross-section, in the shapes different from cylindrical and loaded with wind have not been developed. Eurocode EN 1991-1-4 CEN (2005) does not cover complex structures based on circular cylinders. The reference surface and drag coefficient such structures are difficult to estimate. More important is that additional horizontal force perpendicular to the aerodynamic drag acts on objects in the shape of a curved pipe, which cannot be estimated by Eurocode.

A three dimensional helical structure was analyzed in (Rashidi *et al.* 2012). A wind speed amplification coefficient was determined for a helical structure of 6.7 m outer diameter. A postulated wind speed was of 4.47 m/s.

When it comes to objects studied in this work, the

height of some examples of water slide constructions can reach 25-35 m, with one ascending tower serving several slides as a starting point (see Fig. 1). Such structures have a vertical static system, with horizontal cantilever or strutted beams connected to the columns which in a statical sense are elements with blocked degrees of freedom. The resulting bending moments at the level of the foundation pillars are heavily involved in complex stress analyses of such structures.

In this paper the influence of strong winds is considered on the structures with complicated shape which to some extent are similar to torus. In such a situation strong wind inference caused by the flow around different parts of the same body appears.

Therefore, the aim of the analysis is to test the possibility of a much faster estimation wind loads acting on a fragment of a structure of more complex, curved shape (e.g., water slide) using a simplified model (in the shape of a torus). For this purpose, flow at high speed around a helix, arranged both near a planar surface and high above it, is analyzed. A calculation error is evaluated for this approach. This paper presents a study on development and verification of numerical models of flow at high Reynolds numbers around structural elements with a circular cross-section and simple or nontypical shapes, allowing determination of useful engineering parameters (such as aerodynamic forces, pressure distribution, and air velocity field) impossible to be obtained on the basis of the existing standard EN 1991-1-4 (the so-called wind standard) (CEN 2005).

In the papers: Padewska (2016), Padewska *et al.* (2015), results of numerical analyses were shown and formulas to estimate aerodynamic forces of the object in the shape of a curved pipe (whole or any fragment of the torus) were

<sup>\*</sup>Corresponding author, Ph.D.

E-mail: [agnieszka.padewska-jurczak@polsl.pl](mailto:agnieszka.padewska-jurczak@polsl.pl)

<sup>a</sup>Ph.D.,

E-mail: [piotr.szczepaniak@polsl.pl](mailto:piotr.szczepaniak@polsl.pl)

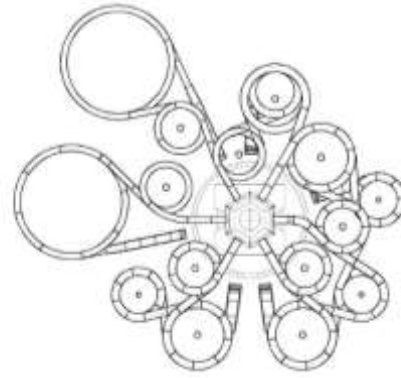


Fig. 1 General view and view of the top of the water slide at Gino Paradise Bešeňová in Slovakia

proposed, depending on: the angle of deviation from the horizontal plane, horizontal wind velocity, radius  $R$  of the torus and the diameter of the cross-section of the track  $b$ . Verifications of obtained formulas were made using additional numerical models. During these estimations, *Finite Element Method* (FEM) and *Finite Volume Method* (FVM) were used. Then, different ways for determining wind forces were described, namely: force transfer in the ANSYS package, *fluid-structure interaction* in Abaqus/CFD package and *User-Defined Functions* (UDF). FSI is a method for analyzing interaction of a structure with surrounding fluid flow. Calculations were carried out in the PL-Grid Infrastructure. In this paper *Finite Volume Method* (FVM) was used to calculate the total wind force acting on an object in the shape of a torus and a helix.

Computation of such a complex case as flow around a helix is very difficult. Fine grid of more than 10,000,000 spatial cells was created. Infrastructure PL-Grid, composed of Computer Centers with supercomputer systems, was used. However, e.g., at 8 parallel processes and 128 GB RAM it allowed to count only 6 seconds of flow in 4 days.

Numerical models of air flow around cylindrical objects are shown. This is a basic model for verifying accepted assumptions. Based on this model, more complex models are created: first in the shape of half of a torus, next in the shape of a helix. Then, results of calculations are presented. Finally, the work is summarized.

## 2. Numerical models of air flow around structural elements

### 2.1 Numerical models of air flow around a cylinder

The development and verification of models of flow around cylindrical elements perpendicular to the direction of wind were presented in previous works (Padewska 2016, Padewska *et al.* 2014). They also include the results of numerical analyses.

Computational domains of rectangular shapes and planar (2D) were prepared in package ANSYS Workbench. In addition, for comparison purposes, other models were made: cylindrical, spatial (3D) and spatial with one layer of grid elements along the length of the cylinder (2.5D) in Abaqus/CFD. The results of numerical analyses are almost

similar, considering the numerical model of air flow in the shape of a rectangle or a circle (see Fig. 2). The diameter of the cylinder is  $b = 1.0$  m. This is a typical dimension of a track of a water slide.

As described in (Padewska *et al.* 2014), air with a constant velocity profile enters the rectangular domain through a front surface (*inlet*) and flows out through the back surface (*outlet*), where the pressure is equal to that of the atmosphere. *Symmetry* (or *far-field* in Abaqus/CFD), which is essentially a *wall* with slip condition, is chosen for the top and bottom boundaries to reduce the computational time. *Inlet* boundary condition is chosen around the perimeter of the circular domain. The roughness of the wall of the cylinder with a value of  $k = 0.15$  mm, which corresponds to the surface of a fiberglass laminate, is considered. As well as adjusting to zero air velocity in the immediate vicinity of the fluid with the surface of the object (*No Slip Wall*). An important issue is the selection of appropriate size of a domain, simultaneously keeping in mind that the calculations are complex, requiring considerable computing power. The computational model dimensions are chosen such that the *inlet*, *outlet*, and *symmetry* or *far-field* boundaries are far enough from the cylinder's surface to avoid any boundary effects, according to (Blocken and Carmeliet 2004), (Blocken and Gualtieri 2012), (Tominaga *et al.* 2008), ANSYS Inc. (2013); Dassault Systemes (2010), Jiyuan *et al.* (2008). The fluid is modeled as an incompressible Newtonian fluid.

Finally, the following computational methods (options) are selected (among others): *pressure-based* solver, *Second-Order Upwind* interpolation scheme, and *transient* flow.

Time step size was also estimated from

$$\Delta t = \frac{b}{n \cdot Sr \cdot w}, \quad (1)$$

The Strouhal number for flow past cylinder is roughly  $Sr = 0.2$ . In order to capture the shedding correctly, in one shedding cycle should be at least  $n = 20$  time steps. In this paper time step size equal 0.002 s is applied. The 10-fold reduction of  $\Delta t$  resulted in no change in the aerodynamic forces values.

Re values applied in calculations were in critical and supercritical ranges of the turbulent flow ( $7.3 \cdot 10^5$ ;  $10^6$ ;  $1.5 \cdot 10^6$  and  $2.2 \cdot 10^6$ ). In particular, the subject of research in

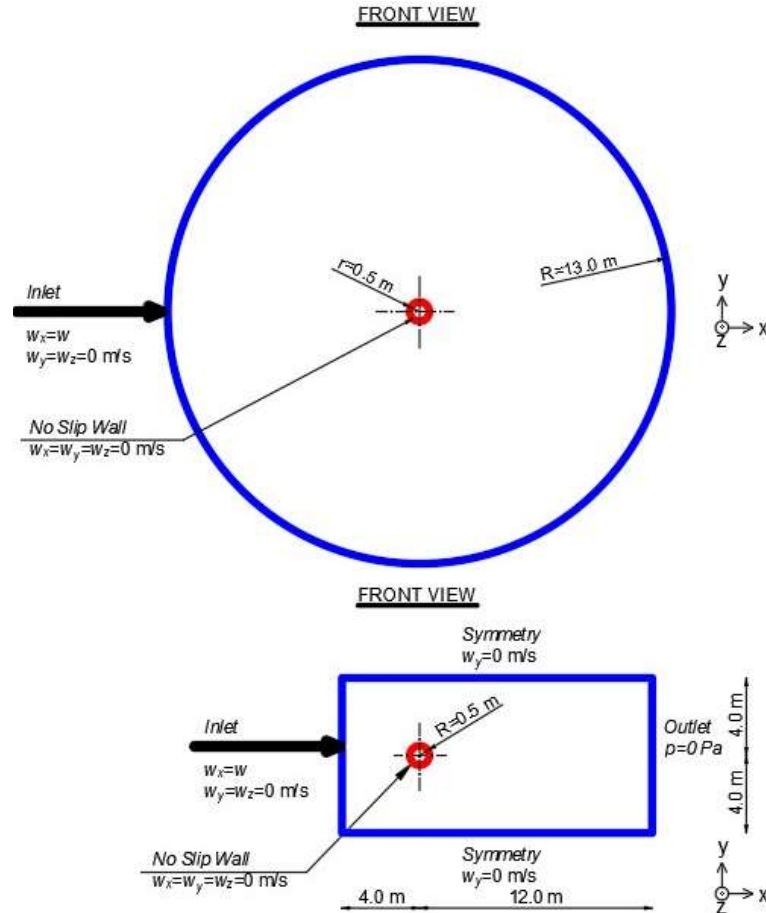


Fig. 2 Dimensions and boundary conditions of a circular and a perpendicular model of air flow around a cylinder

 Table 1 Summary of the  $Re$  values and FVM grid refinements

$w$ [m/s]	11 (strong breeze)	15 (high wind, moderate gale)	22 (strong gale)	33.5 (hurricane)
$Re$ [-]	$7.3 \cdot 10^5$	$10^6$	$1.5 \cdot 10^6$	$2.2 \cdot 10^6$
$y^+$ [-] minimum	6	7	10	14
$y^+$ [-] coarse mesh	50	63	90	135
$y^+$ [-] fine mesh	6	7	40	50

these studies is the air flow around the torus at wind speed  $w = 33.5$  m/s and  $Re = 2.2 \cdot 10^6$ .

The shear-stress (*SST*)  $k-\omega$  turbulence model is chosen. This model is more accurate and reliable for a wider class of flows (e.g., adverse pressure gradient flows, airfoils, transonic shock waves), according to ANSYS Inc. (2013). It blends the robust and accurate formulation of the  $k-\omega$  model in the near-wall region with the freestream independence of the  $k-\varepsilon$  in the far field.

The integral time-average value of the drag coefficient (Padewska *et al.* 2014) using (1) the standard  $k-\omega$  and  $k-\varepsilon/RNG$  turbulence models results in  $c_x^{cylinder} = 0.64$  and (2) the  $k-\omega/SST$  or *DES* models –  $c_x^{cylinder} = 0.59$ . Average value of  $c_y$  is equal to zero. The amplitude of oscillation is 0.3. This value is consistent with the results obtained in the wind tunnel and described in Lienhard (1966).

Table 1 shows, depending on the speed of wind flow

and  $Re$  number, the nondimensional wall distance  $y^+$ , adopted according to Anderson (1995), ANSYS Inc. (2013), Jiyan *et al.* (2008), Versteeg and Malalasekera (2007), Wilcox (2006). In the mentioned references, among others, possible to use ranges of values  $y^+$  are included, corresponding to each zone of the viscosity-affected region. The paper (Suga *et al.* 2005) also reports the development of a refined wall-function strategy for the modelling of turbulent flow over rough surfaces.

Various types of *FVM* meshes were made: structural (Fig. 3(a)), hybrid, or nonstructural. Results of the drag coefficient lead to the conclusion that for calculations and analyses, a structural grid should be chosen if possible. Models have significantly lower computational requirements (and coarse mesh) when wall functions are used. Minimal values of  $y^+$  and  $Re$  values are shown in Table 1 (assuming that the value of  $y$  is slightly greater than

that of  $k$ ). It also includes the maximum values of  $y^+$  (a fine mesh) for which the drag coefficients remain almost unchanged, it means that difference between solutions for different small  $y^+$  is less than 5% (according to Fig. 3(b)—which shows the results of the analysis of the sensitivity of the drag coefficient depending on grid refinement and wind speed—part of curves for  $y^+$  from the range 0–50). Larger values of  $y^+$  than those listed in Table 1 do not apply in these analyses.

The maximum values of  $c_x$  coefficients for models with a coarse mesh are comparable (lower by about 5%—see Fig. 3(c) - an upper line) with the force coefficients values given in the European code CEN (2005). Following the adoption of more restrictive rules of discretization, drag coefficient values proved to be lower by about 30%, and they are consistent with the results measured in the

cryogenic wind tunnel and described in Adachi (1995).

As described in Padewska *et al.* (2014),  $y^+ > 135$  for  $w = 33.5$  m/s and  $y^+ > 50$  for  $w = 11$  m/s (except for the front and the trailing surface of the cylinder, where stagnation of air occurs). Such values were adopted during creation of a coarse grid (Table 1). Furthermore, it does not drop significantly below 50 for  $w = 33.5$  m/s and below 6 for  $w = 11$  m/s, which are equal to  $y^+$  values for a fine grid (Table 1). Therefore, it can be concluded that the near-wall mesh resolution is acceptable.

Behind the cylinder is the region in which air recirculates. A similar angle was determined experimentally and described in Roshko (1960). Furthermore, a very good agreement is observed between the results of the mean pressure distribution on the cylinder surface at  $Re = 2.2 \times 10^6$  in this paper (Fig. 3(d)) and sets of experimental data

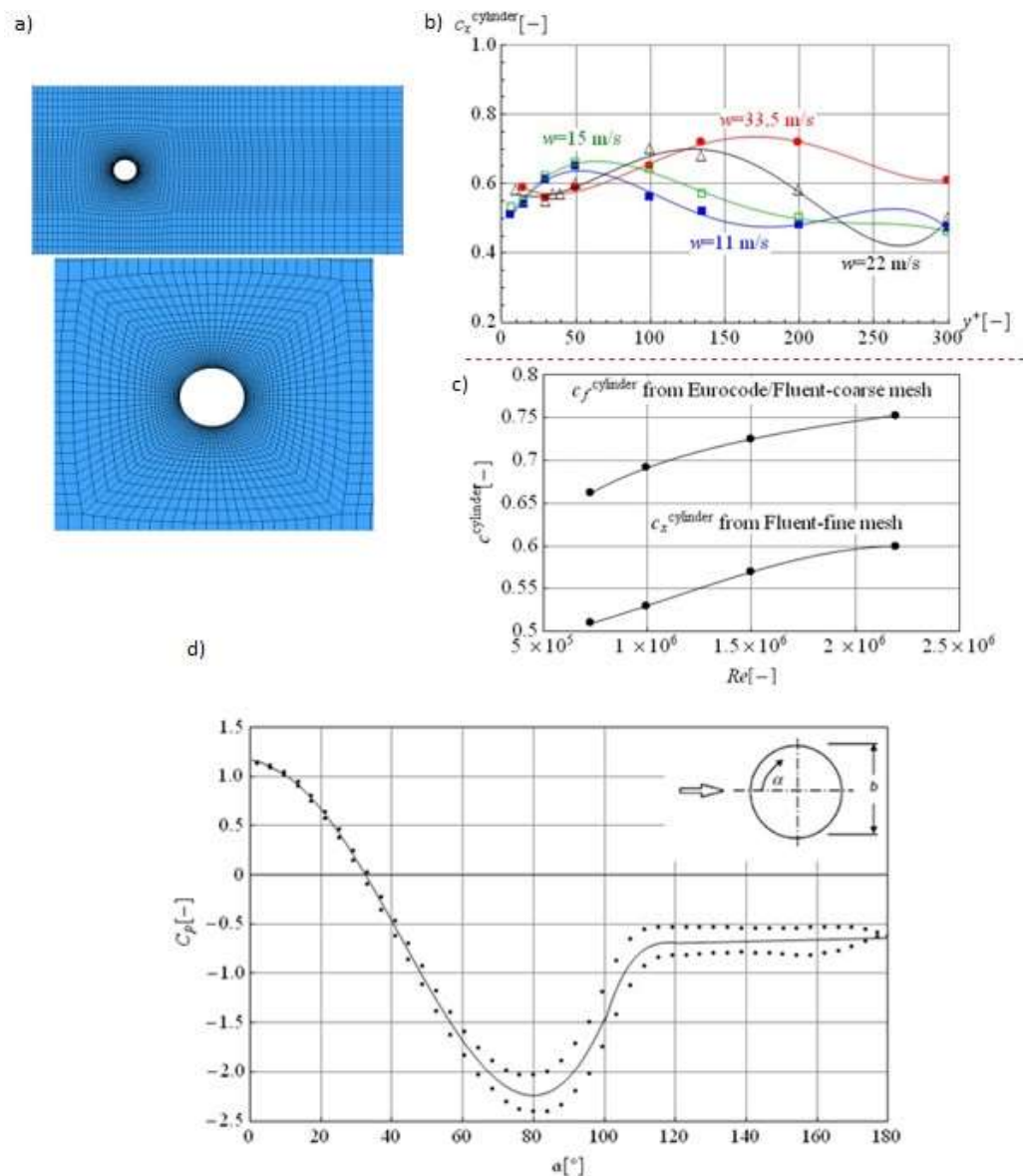


Fig. 3 (a) structural fine FVM mesh of the base model of flow around a cylinder in the entire domain and a layer near the wall of the cylinder, (b) drag coefficients according to grid refinements at different air velocities, (c) variations of drag and force coefficients with the Reynolds number for the value of equivalent surface roughness  $k = 0.15$  mm and (d) distribution of average values of pressure coefficient  $C_p$  on the wall of the cylinder

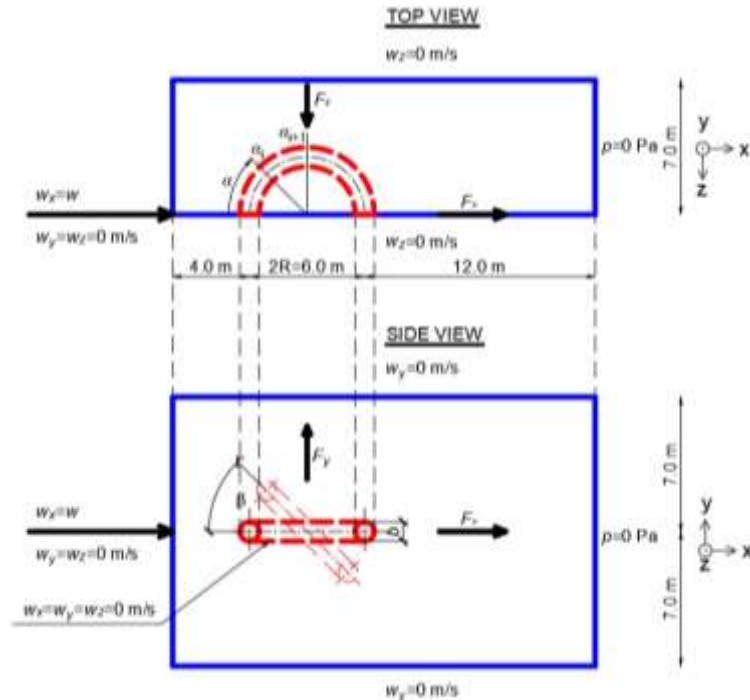


Fig. 4 Boundary conditions and directions of aerodynamic forces in a model of flow around half of a torus

described in Jones and Cincotta (1969), Roshko (1960), Warschauer and Leene (1971), Zdravkovich (1997), and also numerical results in Catalano *et al.* (2003), Yeo and Jones (2011) and data described in European code CEN (2005). A similar distribution of pressure coefficients were obtained for the other Re numbers:  $7.3 \cdot 10^5$ ,  $10^6$ , and  $1.5 \cdot 10^6$  (Padewska *et al.* 2015, 2014).

Additional *FSI* analysis are performed in the Abaqus package to determine the aerodynamic forces. *FSI* represents a class of multiphysics problems where fluid flow affects compliant structures, which in turn affects the fluid flow (Bazilevs *et al.* 2013). Boundary conditions are almost the same as in ANSYS, but *far-field* is chosen for the top and bottom surfaces. It is assumed that the element does not deform under the influence of wind and it does not moves. Considering the turbulence model *k-omega/SST* in ANSYS Fluent, a value of drag coefficient close to the value resulting from the application of the model *k-epsilon/RNG* in the Abaqus package is obtained, regardless of the method specified in EN 1991-1-4 (CEN 2005).

Following the adoption of all previous rules, the problem is converged. Residuals are decreased by three orders of magnitude. The net mass imbalance is less than 0.2% of the net flux through the domain. It means that when using present models, reliable results are obtained.

Selected models will be used as a base for further analysis, as described in the following sections of this paper.

## 2.2 Assumptions and numerical models of air flow around half of a torus

The development and verification of models of wind flow around the spatial elements in the shape of half of a torus, inclined at the angle  $\beta$  in the range  $0-90^\circ$  were shown

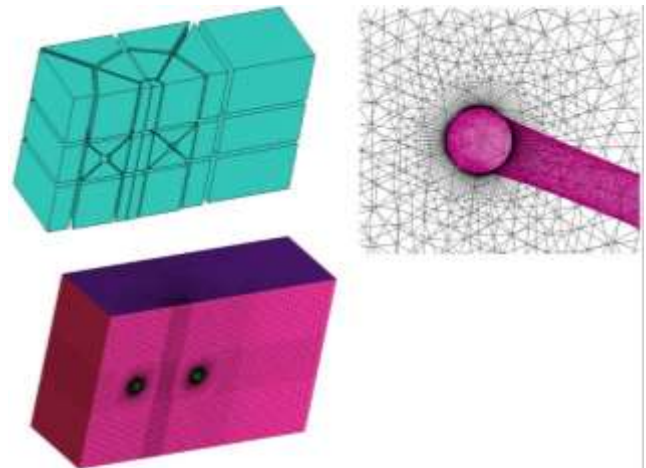


Fig. 5 Division into blocks, structured FVM mesh and unstructured FVM mesh in the vicinity of a wall of the model of flow around a curved pipe

in previous papers.

Figs. 4 and 5 show boundary conditions, directions of aerodynamic forces, division into blocks and *FVM* mesh of the numerical model of air flow around the object in the shape of half of the torus, made in the ANSYS package.

In particular, the subject of research in these studies is the air flow around the torus at an angle  $\beta = 0^\circ; 22.5^\circ; 45^\circ$  and  $90^\circ$  and total aerodynamic forces. The radius of the torus  $R = 3.0$  m, and the diameter of the cross-section of the track  $b = 1.0$  m. Boundary conditions and mesh in the region of boundary layer are the same as in the case of the base, cylindrical model. A turbulence model *k-omega/SST* is adopted with the same parameters as during the modeling of the base model.

Sometimes the division into blocks is difficult. In those cases, hybrid grid or unstructured grid is performed. This resulted in a prolongation of the calculation time from several hours to more than 17 hours in the Polish Grid Infrastructure. Analysis of flow around a helix (see Section 2.3) will force the use of unstructured grid formed of prisms (wedges) near the wall of the pipe and tetrahedrons in the area away from it. The boundary layer is discretized in a similar manner as in the case of the base model, according to Table 1, using a fine mesh composed of more than 1,741,000 spatial elements. A comparison of the results for a model of half of the torus inclined from the horizontal surface at  $22.5^\circ$  shows that the forces  $P_x$  and  $P_z$  obtained using hybrid and unstructured grids do not differ by more than 2%.

An analytical approach to the problem was proposed in Szczepaniak and Padewska (2014). In order to simplify the manual calculations, the total effects of the axis curvature and rotation have been compressed into a single vector coefficient  $\boldsymbol{\mu}$ , named the position coefficient, which can be used in the following manner

$$\mathbf{F}_{w0} = \frac{\mathbf{F}_w}{c_s c_d} = q_p \cdot c_{f,0} \cdot A_{\text{ref}} \cdot \boldsymbol{\mu} = q_p \cdot c_{f,0} \cdot b \cdot l \cdot \{\mu_x; \mu_y; \mu_z\}^T, \quad (2)$$

where  $\mathbf{F}_{w0}$  is the wind force vector (without the effects of the structural coefficient  $c_s c_d$ )—[N];  $q_p$  is the peak air velocity pressure—[Pa];  $c_{f,0}$  is the force coefficient;  $b$  is the diameter of the cylinder—[m];  $l$  is the length of the axis of the element [m];  $\mu_x$ ,  $\mu_y$ , and  $\mu_z$  are the longitudinal, lateral,

and vertical components of the position coefficient  $\boldsymbol{\mu}$ . The distribution of position coefficients for sloped torus was presented in Szczepaniak and Padewska (2014), as well.

Exemplary relationships describing the change of resultant aerodynamic forces  $P_x$  and  $P_z$  were shown in (Padewska 2016, Padewska *et al.* 2015). Results of numerical analyses, using force transfer and User Defined Functions (UDF), were shown and formulas to estimate aerodynamic forces of the object in the shape of a curved pipe (whole or any fragment of the torus) were proposed, depending on: the angle of deviation from the horizontal plane, horizontal wind velocity, radius  $R$  of the torus, the diameter of the cross-section of the track  $b$  and part of a torus. Parameters values necessary for determining the velocity and impact of the wind were calculated in accordance with the formulas in the European standard CEN (2005). These forces can be estimated by

$$P_x = c_f q_p b R \zeta_x, \quad (3)$$

$$P_z = c_f q_p b R \zeta_z. \quad (4)$$

In the formula values  $c_f$  and  $q_p$  according to standard CEN (2005) shall be substitute, angles expressed in degrees and coefficients  $\zeta_x$ ,  $\zeta_z$  presented in (Padewska 2016). Derived formulas include appropriate safety margin. Drag force of any part of a torus can be estimated from

$$P_x = P_x(\alpha_{2,2}) - P_x(\alpha_{2,1}). \quad (5)$$

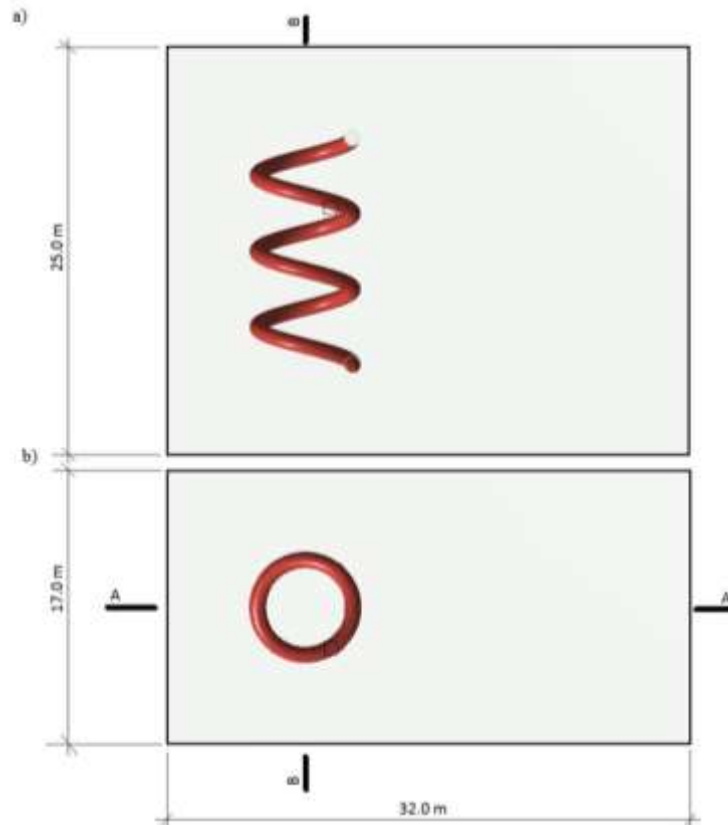


Fig. 6 Dimensions of a computational domain with a helix positioned high above a horizontal surface (a) front view; and (b) top view

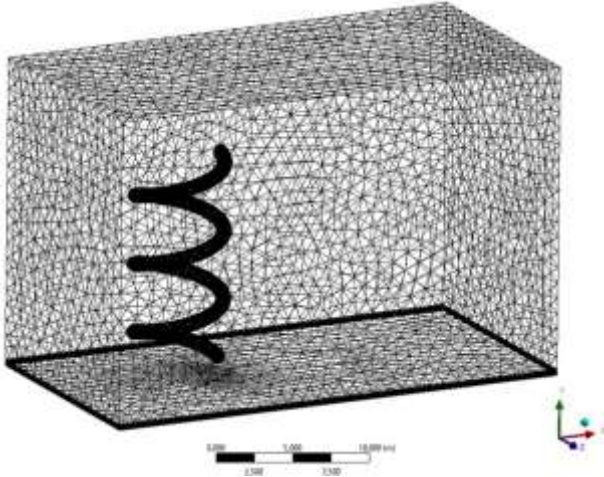


Fig. 7 FVM grid of a model of air flow around a helical object positioned near a horizontal surface

More accurate dependencies were obtained for a whole object

$$P_x = c_f q_p b R [2,21 - 0,97 \arctan(2,098 - 0,034\beta)] \quad (6)$$

$$P_z = c_f q_p b R [(-0,91 + 0,31 \arctan(4,10 - 0,07\beta))] \quad (7)$$

At this stage of the test, formulas are correct with respect to curved pipes with  $R/b = (3.0 - 13.0)$  and the diameter of the running track  $b = (0.8 - 1.0)$  m.

### 2.3 Assumptions and numerical models of air flow around a Helix

The model in the shape of a helix in ANSYS Fluent consists of one part (wind flow with cutout in the shape of helix); however, “in thought” a structural element can be divided into six halves of a torus with a radius of  $R = 3.0$  m, inclined from the horizontal surface by the angle  $22.5^\circ$ . Wind speed  $w = 33.5$  m/s.

A turbulence model *SST k- $\omega$*  with the same parameters as in the case of the base model is adopted. Boundary conditions are the same as in the case of a spatial model of the whole torus or its half. Wind velocity is constant at inlet. Fig. 6 shows views from the front and top of the model. In the second step of the analysis the model of the helix is moved closer to a distance of 1 m from the bottom planar surface on which the *No Slip Wall* boundary condition is declared. The effect of surface roughness to reduce the speed in the case of the body located near the planar surface was investigated. The logarithmic profile of wind speed was obtained from numerical calculations. It turned out that reduced speeds do not have a significant impact both on the construction of the high altitude and horizontal structural elements, which are located at a high altitude above the ground level.

In the Fig. 7 the discretized model of a fragment of a water slide arranged near a planar surface with the unstructured mesh *FVM* is illustrated. Near the bottom surface, the grid is thickened (thick black line in Fig. 7).

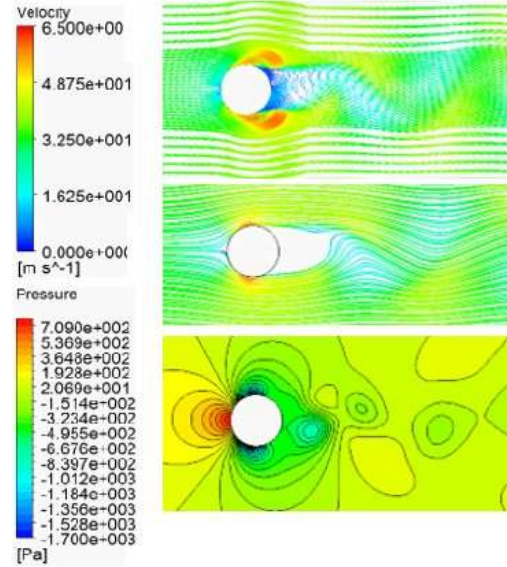


Fig. 8 Fields of: velocity, streamlines and pressure at time step 9 s,  $Re = 2.2 \times 10^6$

The boundary layer near the wall is also discretized in a similar manner to the base case model, according to Table 1, using fine grid of more than 10 000 000 spatial cells. Calculations were carried out in the PL-Grid Infrastructure.

## 3. Results of calculations

### 3.1 Results of calculations of air flow around a cylinder

Distribution of, respectively, velocity, streamlines, and pressure at time step 9 s, determined from numerical analyses at hurricane wind speed are shown in the Fig. 8. The air flow is inhibited directly in front of the body. A high value of overpressure appears in this place, whereas for the remaining points on the windward surface of the cylinder, the pressure is smaller, as the flow is not completely inhibited. The airflow, in accordance with the equation of continuity, must accelerate on both sides of the body. Therefore, the static pressure on the upper and lower surfaces of the cylinder drops. On the trailing surface of the cylinder, the pressure remains approximately constant. Vortices are created at the back of the body that detach periodically from either side of the body. The flow behind the cylinder is unsteady, turbulent, swirling, and asymmetrical. Just behind the cylinder, streamlines are approximately parallel to the direction of the velocity of the incoming stream, and stagnation of air occurs in this region. Results are similar to those in (Van Dyke 1988). The figure shows that the *CFD* numerical analysis are able to give the characteristics of the “real” flow: separation of the stream and creation of two large vortices, as well as more dispersed turbulent vortices in the vortex street. Similar results were achieved in Perrin *et al.* (2007), Lysenko *et al.* (2013), Robertson *et al.* (2015), Yuan *et al.* (2018) or Salvatici and Salvetti (2003).

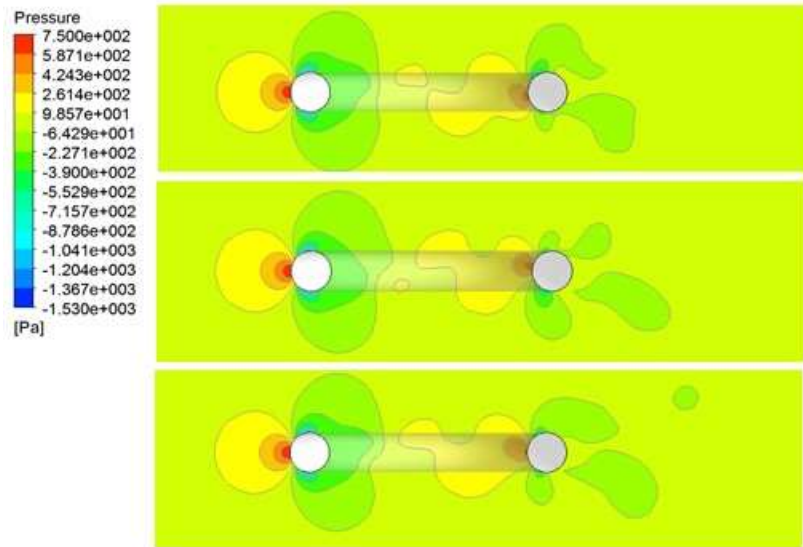


Fig. 9 Pressure distribution around half of the torus arranged horizontally at hurricane wind speed at the time when the resultant aerodynamic drag force reaches consecutively minimum, mean and maximum values

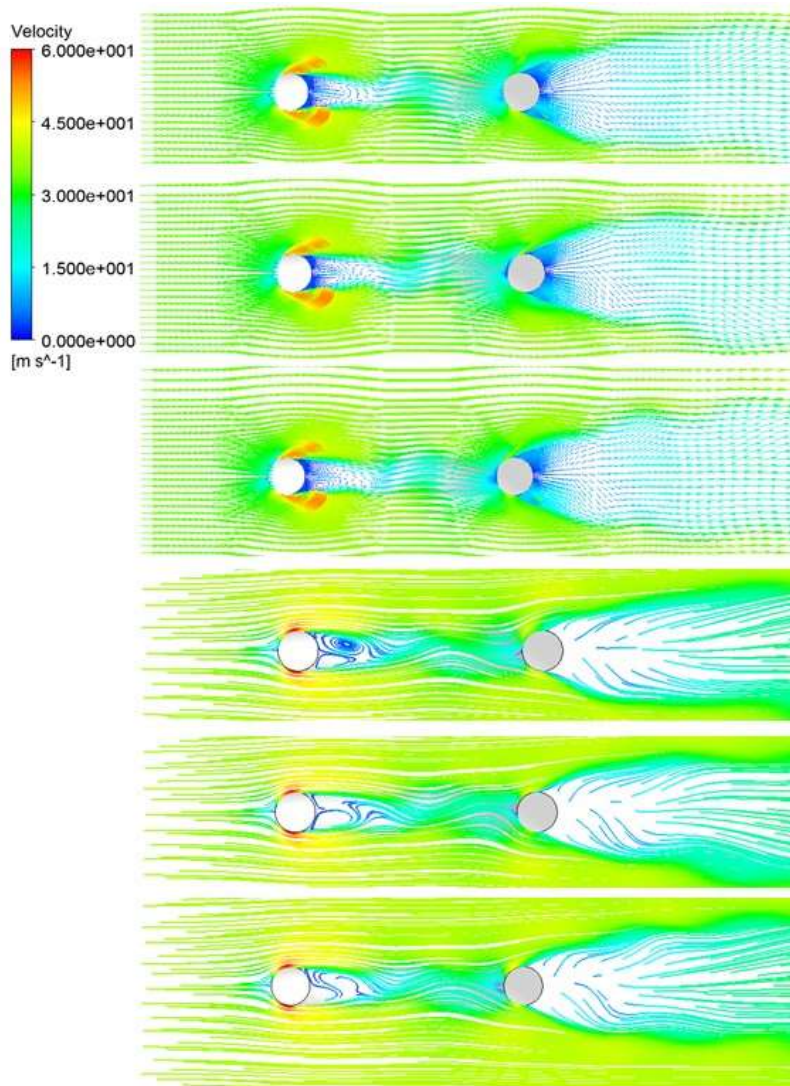


Fig. 10 Velocity and streamlines distribution around half of the torus arranged horizontally at hurricane wind speed at the time when the resultant aerodynamic drag force reaches consecutively minimum, mean, and maximum values

### 3.2 Results of calculations of air flow around half of a torus

The subject of analysis are reactions of the torus due to changes in the flow characteristics, for example, pressure. Figs. 9 and 10 illustrate the changes in pressure, velocity, and streamlines around half of the torus arranged horizontally at hurricane wind speed at the time when the resultant aerodynamic drag force reaches consecutively minimum, mean, and maximum values. The drawings have been trimmed for better visibility. Partial results have already been presented in earlier works (Padewska 2016).

They show that in the case of a torus in a horizontal position in the front view, a path of disturbed flow is created behind a windward quarter (see Figs. 9 and 10). Pressure and velocity distributions are almost constant in time. The turbulent boundary layer separation point is located at the back. The value of the drag coefficient decreases. Vortices are formed almost symmetrically. The flow behind the leeward quarter of the torus is unsteady, swirling, asymmetrical, chaotic, and random. Pressure and velocity distributions change rapidly in time. This is the supercritical range of the Re number ( $Re > 2.0 \cdot 10^6$ ).

Calculations carried out in the program Abaqus/CFD

confirm that the flow near the leeward part of the half torus is turbulent. Streamlines are arranged in a similar manner. Finding references about experimental research of flow around an object in the shape of a torus was very problematic (authors found no research relevant to the scope of the present work). It is similar to experimental visualization of flow around two cylinders spaced from each other at a distance  $L/D = 4.0$ , where  $L$  is the distance between the cylinders [m] and  $D$ —diameter of the cylinder [m], according to Su and Zhang (2004). Also in this case, random and turbulent flow in the vicinity of the leeward cylinder is notable.

The effect of a turbulent and random flow around the leeward part of a half torus inclined from the horizontal plane at an angle  $\beta = 45^\circ$  is maintained, as shown in Fig. 11. Thus, a considerable impact of the curvature of the axis of the torus on the pressure and velocity distributions in the whole object is shown. The research in (Padewska 2016) shows that in the case of two cylinders set at an angle of  $\beta = 45^\circ$  to the wind direction and spaced from each other by a distance comparable to twice the radius of the  $R$ -torus, this effect disappears.

Separate paths of vortices, viewed from the front, are visible at the vertical arrangement of half of the torus and at

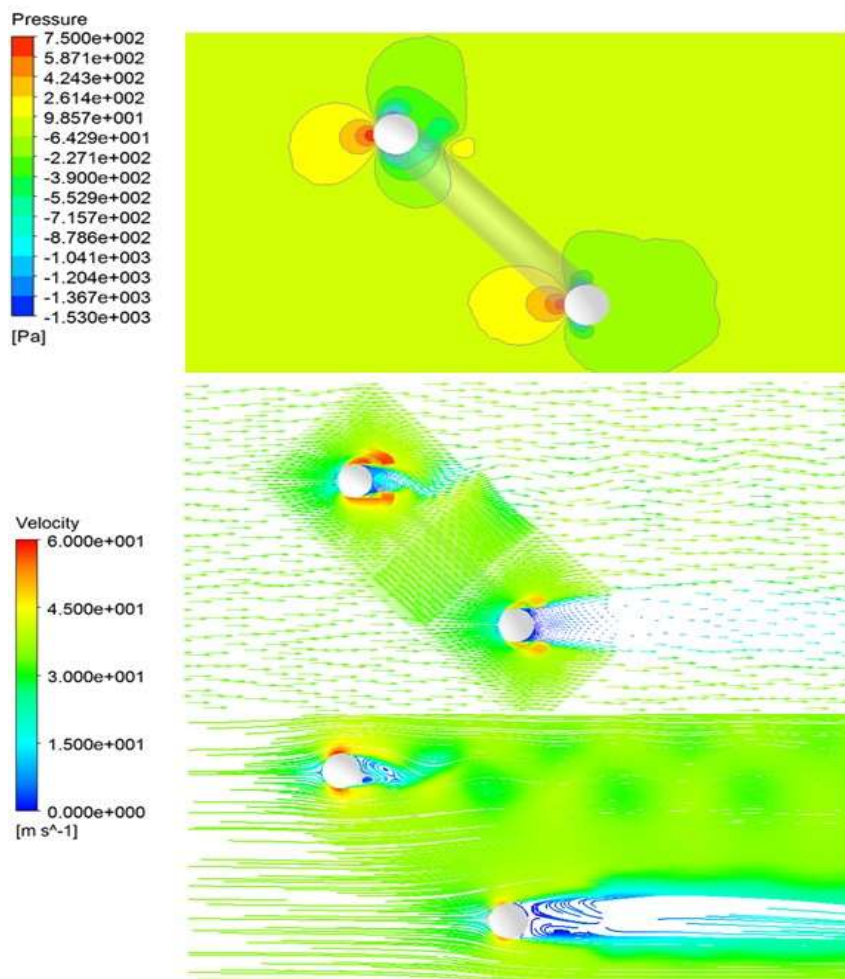


Fig. 11 Distribution of pressure, velocity, and streamlines around half of a torus inclined at an angle  $\beta = 45^\circ$  at  $w = 33.5$  m/s

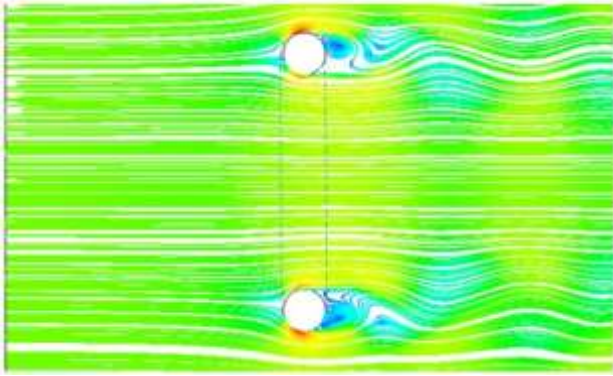


Fig. 12 Streamlines around half of a torus in vertical position at  $w = 33.5$  m/s

a horizontal direction of air velocity (see Fig. 12).

Similar pressure and velocity distributions were also observed at lower values of wind speed (11 m/s, 15 m/s and 22 m/s).

Fig. 13 shows the distributions of pressure, velocity, and streamlines in the middle cross-section of the model of flow around half of the torus. The largest absolute value of the lateral (side) force directed outwardly relative to the axis of the curvature of the torus appears on 5<sup>th</sup> and 6<sup>th</sup> parts of the torus (see Fig. 4; the angle  $\alpha$  of approximately  $110^\circ$ ). Its source is a big difference between the air velocity in the region in the “eye” (the center) of the torus and on sides. The effect is analogous to the lift force obtained by airfoils. (Noorani *et al.* 2013) observed that for strong curvature a distinct bulge appears close to the pipe centre in fully

developed, statistically steady turbulent flow in straight and curved (a fragment of a torus) pipes at moderate Reynolds numbers.

### 3.3 Results of the calculations of air flow around a helix

Shown in the Fig. 14 fields of pressure, velocity, and streamlines around an object in the shape of a helix positioned high above a flat surface, justify that wind load acting on a fragment of a structure of a more complex curved shape (e.g., water slide) may be tested by a simplified model.

Results were read when the drag coefficient reached the integral time-average value, but it can be roughly assumed that this value is almost unchanged over time. Vertical, middle cross-section A-A through an object is selected (see Fig. 6). The drawings have been trimmed for better visibility.

Behind the windward part of the object flow is disturbed as in the case of the torus. The turbulent boundary layer separation point is located at the back. The effect of turbulent and random flow around the leeward parts of the object is maintained as shown in Fig. 14. Thus, a considerable impact of the curvature of the axis of the helix on the pressure and velocity distributions in the whole object is shown. However, the division of areas in which wind pressure or wind suction acts around the leeward part of the pipe is clearer than that in the case of the torus positioned horizontally. The drag coefficient increases.

Fig. 15 shows a static pressure distribution on the wall of the object in the shape of a helix. It is similar to the

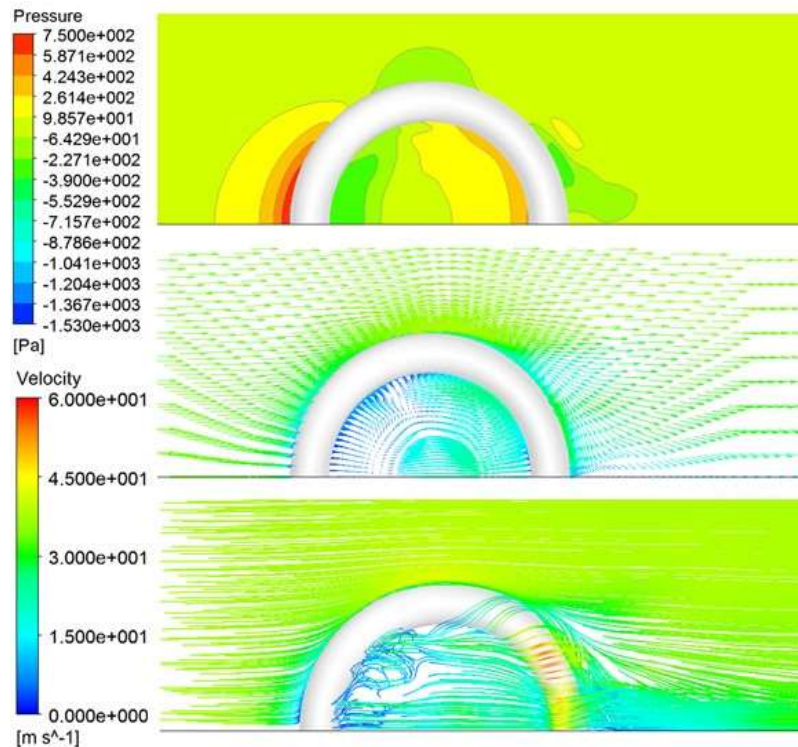


Fig. 13 Distribution of pressure, velocity and streamlines in the middle cross-section of a model of flow around half of the torus at  $\beta = 0^\circ$  and  $w = 33.5$  m/s

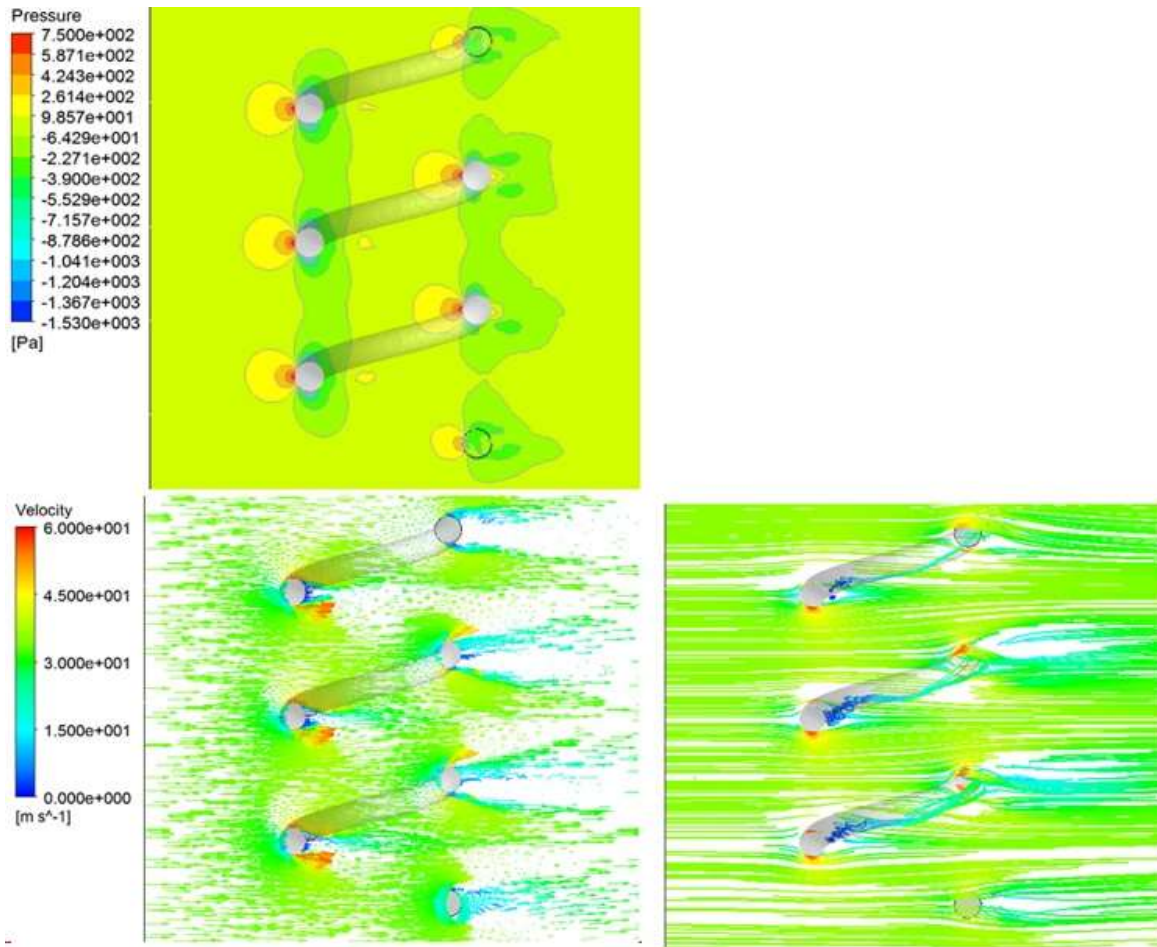


Fig. 14 Pressure, velocity and streamlines distribution around a helical object positioned high above a planar surface in A–A cross-section

pressure distribution on the wall of half of a torus inclined from the horizontal surface by an angle  $22.5^\circ$ .

Furthermore, the pressure, velocities and streamlines fields in the most part of the computing domain remain nearly identical when the object is moved closer to the horizontal surface. Only in area very close to the ground a logarithmic velocity profile is created due to friction. However, it does not have a significant effect on the aerodynamic forces, except for the viscosity.

The highest values of drag force are observed on the front and rear parts of the half torus. The total aerodynamic drag of a helical object at hurricane wind speed is about 4% less than 3 times the drag of a single torus, whereas  $P_z$  forces are equal to zero. As previously noted, the impact of air friction at the ground on values of wind force (except viscosity) is negligible, as the value of drag of the object located high above the planar surface is about 3% less than the resistance of the helix positioned close to the surface. In the section B–B (see Fig. 16) and thus in a direction perpendicular to the wind velocity, there is no clear detachment of air streams.

Therefore, it is possible to divide a more complex object (e.g. in the shape of a helix) into simpler elements (toruses) to estimate aerodynamic forces. These forces can be determined by earlier proposed formulas relating to objects in the shape of a torus. The derived formulas include

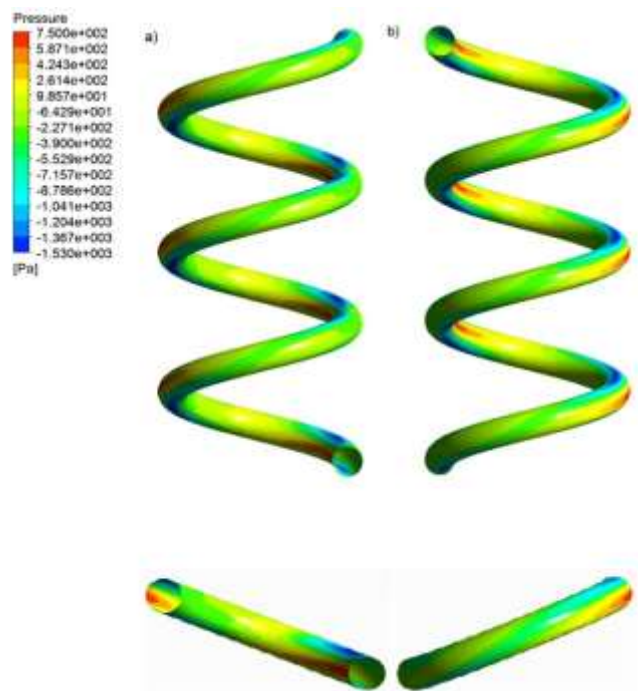


Fig. 15 Pressure distribution on a surface of a helix and a torus: (a) front view and (b) rear view

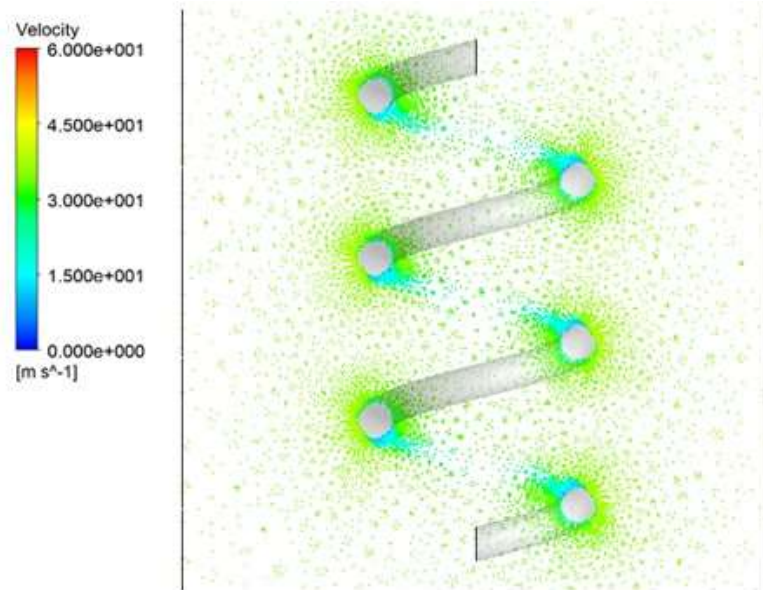


Fig. 16 Velocity distribution around a helical object positioned high above a planar surface in B–B cross-section

appropriate safety margin. The conclusions also apply to smaller wind speed (11 m/s; 15 m/s and 22 m/s).

#### 4. Conclusions

The aim of the analysis was to test the possibility of a much faster estimation wind loads acting on a fragment of a structure of more complex, curved shape (e.g., water slide) using a simplified model (in the shape of a torus). The division of complex structures into parts is necessary, especially in the case of engineering tasks carried out by small teams. For this purpose, flow at high speed around a torus and helix was analyzed.

The first stage of the research concerned calculations of flow around circular cylinders with a diameter  $b = 1.0$  m in ANSYS package. Next analyzes involved models of wind flow around the spatial elements in the shape of half of a torus and a helix (six halves of a torus).

In the case of a torus in a horizontal position and inclined from the horizontal plane at an angle  $\beta = 45^\circ$  a considerable impact of the curvature of the axis of the torus on the pressure and velocity distributions in the whole object was shown. A path of disturbed flow was created behind a windward quarter. The flow behind the leeward quarter of the torus was unsteady, swirling, asymmetrical, chaotic, and random. Separate paths of vortices, viewed from the front, were visible at the vertical arrangement of half of the torus and at a horizontal direction of air velocity.

The largest absolute value of the lateral (side) force directed outwardly relative to the axis of the curvature of the torus appears on 5<sup>th</sup> and 6<sup>th</sup> parts of the torus (the angle  $\alpha$  of approximately  $110^\circ$ ). Its source is a big difference between the air velocity in the region in the “eye” (the center) of the torus and on sides.

Fields of pressure, velocity, and streamlines around an object in the shape of a helix positioned high above a flat surface, justify that wind load acting on a fragment of

a structure of a more complex curved shape (e.g., water slide) may be tested by a simplified model using obtained in previous works mathematical relationships. Pressure and velocity distributions around an object in the shape of a helix was similar to the pressure distribution around half of a torus. Formulas include appropriate safety margin. At this stage of analyses, formulas are correct with respect to curved pipes with  $R / b = (3.0 - 13.0)$  and the diameter of the running track  $b = (0.8 - 1.0)$  m.

#### Acknowledgments

This research was supported in part by the PL-Grid Infrastructure. Thanks to Translmed for proof reading.

#### References

- Adachi, T. (1995), “The effect of surface roughness of a body in the high Reynolds – number flow”, *Int. J. Rotating Mach.*, **2**, 23-32. <https://doi.org/10.1155/S1023621X95000066>.
- Anderson, J. (1995), *Computational Fluid Dynamics. The Basics with Application*, McGraw-Hill, Inc., USA.
- ANSYS Inc. (2013), *ANSYS Documentation for Release 15/Custom Training Material*.
- Bazilevs, Y., Takizawa, K. and Tezduyar, T. (2013), *Computational Fluid-Structure Interaction: Methods and Applications*, John Wiley and Sons, Ltd.
- Blocken, B. and Carmeliet, J. (2004), “Pedestrian Wind Environment Around Buildings: Literature Review and Practical Examples”, *J. Therm. Envelope Build. Sci.*, **28**(2), 107-159. <https://doi.org/10.1177/1097196304044396>.
- Blocken, B. and Gualtieri, C. (2012), “Ten iterative steps for model development and evaluation applied to Computational Fluid Dynamics for Environmental Fluid Mechanics”, *Environ. Model. Softw.*, **33**, 1-22.
- Catalano, P., Wang, M., Iaccarino, G. and Moin, P. (2003), “Numerical simulation of the flow around a circular cylinder at high Reynolds numbers”, *Int. J. Heat Fluid Fl.*, **24**, 463-469.

- [https://doi.org/10.1016/S0142-727X\(03\)00061-4](https://doi.org/10.1016/S0142-727X(03)00061-4).
- CEN (2005), EN 1991-1-4 *Eurocode 1: Actions on structures - Part 1-4: General actions - Wind actions with National Annex*, CEN, PKN, Brussels, Warszawa.
- Dassault Systemes (2010), *Introduction to Abaqus/CFD*. Vélizy-Villacoublay, France.
- Jiyuan, T., Guan, H. and Chaoqun, L. (2008), *Computational Fluid Dynamics. A Practical Approach*, Elsevier Inc., USA.
- Jones, J.G.W. and Cincotta, J. (1969), "Aerodynamic forces on a stationary and oscillating circular cylinder at high Reynolds numbers", Washington.
- Lienhard, J.H. (1966), "*Synopsis of lift, drag, and vortex frequency data for rigid circular cylinders*", Washingt. State Univ. Coll. Eng. Res. Div. Bull. U.S.A.
- Lysenko, D.A., Ertesvåg, I.S. and Rian, K.E. (2013), "Modeling of turbulent separated flows using OpenFOAM", *Comput. Fluids*, **80**, 408-422. <https://doi.org/10.1016/j.compfluid.2012.01.015>.
- Noorani, A., El Khoury, G.K. and Schlatter, P. (2013), "Evolution of turbulence characteristics from straight to curved pipes", *Int. J. Heat Fluid Fl.*, **41**, 16-26. <https://doi.org/10.1016/j.ijheatfluidflow.2013.03.005>.
- Padewska, A. (2016), "Pogłębiona analiza numeryczna oddziaływania wiatru na obiekty budowlane o nietypowym kształcie i układzie", Silesian University of Technology.
- Padewska, A., Szczepaniak, P. and Wawrzynek, A. (2015), "Oddziaływanie wiatru na obiekt o nietypowym kształcie", *Inżynieria i Bud.*, **71**, 381-385.
- Padewska, A., Szczepaniak, P. and Wawrzynek, A. (2014), "Analysis of fluid-structure interaction of a torus subjected to wind loads", *Comput. Assist. Method. Eng. Sci.*, **21**, 151-167.
- Perrin, R., Braza, M., Cid, E., Cazin, S., Barthet, A., Sevrain, A., Mockett, C. and Thiele, F. (2007), "Obtaining phase averaged turbulence properties in the near wake of a circular cylinder at high Reynolds number using POD", *Exp. Fluids*, **43**, 341-355. <https://doi.org/10.1007/s00348-007-0347-6>.
- Rashidi, M., Kadambi, J. and Kerze, D. (2012), "Wind flow regime around a 3 dimensional helical structure", *Proceedings of the ASME 2012 International Mechanical Engineering Congress and Exposition*, Volume 7: Fluids and Heat Transfer, Parts A, B, C, and D. Houston, Texas, USA.
- Robertson, E., Choudhury, V., Bhushan, S. and Walters, D.K. (2015), "Validation of OpenFOAM numerical methods and turbulence models for incompressible bluff body flows", *Comput. Fluids*, **123**, 122-145. <https://doi.org/10.1016/j.compfluid.2015.09.010>
- Roshko, A. (1960), "Experiments on the flow past a circular cylinder at very high Reynolds number", *J. of Fluid Mech.*, **10**(3), 345-356. <https://doi.org/10.1017/S0022112061000950>.
- Salvatici, E. and Salvetti, M.V. (2003), "Large eddy simulations of the flow around a circular cylinder: effects of grid resolution and subgrid scale modeling", *Wind Struct., Int. J.*, **6**(6), 419-436. <https://doi.org/10.12989/was.2003.6.6.419>
- Su, Z.D. and Zhang, H.J. (2004), "Unsteady Incompressible Viscous Flows around Two Circular Cylinders in Tandem", *Proceedings of the 10th Asian Congress of Fluid Mechanics*, Sri Lanka.
- Suga, K., Craft, T.J. and Iacovides, H. (2005), "Extending an analytical wall-function for turbulent flows over rough walls, in: engineering turbulence modelling and experiments", Sardinia, Italy, 157-166. <https://doi.org/10.1016/B978-008044544-1/50014-5>.
- Tominaga, Y., Mochida, A., Yoshie, R., Kataoka, H., Nozu, T., Yoshikawa, M. and Shirasawa, T. (2008), "AIJ guidelines for practical applications of CFD to pedestrian wind environment around buildings", *J. Wind Eng. Ind. Aerod.*, **96**(10-11), 1749-1761. <https://doi.org/10.1016/j.jweia.2008.02.058>.
- Szczepaniak, P. and Padewska, A. (2014), "Wind load of a curved circular cylinder structures", (Eds., Jendzelovsky, N. and Grmanova, A.), *12th International Conference on New Trends in Statics and Dynamics of Buildings*, Bratislava: Slovak University of Technology, Bratislava, Slovakia, **769**, 517-530. <https://doi.org/10.4028/www.scientific.net/AMM.769.172>.
- Van Dyke, M., 1988, *An Album of Fluid Motion*, The Parabolic Press, Stanford, California. USA.
- Versteeg, H. and Malalasekera, W. (2007), *An Introduction to computational fluid dynamics: the finite volume method*, Pearson Education Ltd.
- Warschauer, K. and Leene, J. (1971), "Experiments on mean and fluctuating pressures of circular cylinders at cross flow at very high Reynolds number", *Proc. Int. Conf. on Wind Effects on Buildings and Structures*, Tokyo, Japan, 305-315.
- Wilcox, D. (2006), *Turbulence Modelling for CFD*, DCW Industries, USA.
- Yeo, D. and Jones, N. (2011), "Computational Study on 3-D Aerodynamic Characteristics of Flow around a Yawed, Inclined, Circular Cylinder", Urbana-Champaign.
- Yuan, W., Yu, N. and Wang, Z. (2018), "The effects of grooves on wind characteristics of tall cylinder buildings", *Wind Struct., Int. J.*, **26**(2), 89-98. <https://doi.org/10.12989/was.2018.26.2.089>.
- Zdravkovich, M. (1997), *Flow around Circular Cylinders. Fundamentals, vol.1*, Oxford University Press, UK.

FR